Single-Molecule Phenyl-Acetylene-Macrocycle-Based Optoelectronic Switch Functioning as a Quantum-Interference-Effect Transistor

Liang-Yan Hsu and Herschel Rabitz[*]

Department of Chemistry, Princeton University, Princeton, New Jersey 08544, USA
(Received 10 July 2012; revised manuscript received 19 September 2012; published 31 October 2012)

This work proposes a new type of optoelectronic switch, the phenyl-acetylene-macrocycle-based single-molecule transistor, which utilizes photon-assisted tunneling and destructive quantum interference. The analysis uses single-particle Green's functions along with Floquet theory. Without the optical field, phenyl-acetylene-macrocycle exhibits a wide range of strong antiresonance between its frontier orbitals. The simulations show large on–off ratios (over 10^4) and measurable currents ($\sim 10^{-11}$ A) enabled by photon-assisted tunneling in a weak optical field ($\sim 2 \times 10^5$ V/cm) and at a small source-drain voltage (~ 0.05 V). Field amplitude power scaling laws and a range of field intensities are given for operating one- and two-photon assisted tunneling in phenyl-acetylene-macrocycle-based single-molecule transistors. This development opens up a new direction for creating molecular switches.

Molecular electronics is an active field under theoretical [1–5] and experimental study [6–12] due to the promise of applications in nanoelectronic devices. In order to make practical molecular devices, it is necessary to control electric currents through single molecules by applying external fields, e.g., with gate electrodes [7,9] or optical fields [3,8,11,13–16]. Recent studies consider optical control of current by utilizing photochemical reactions [8], manipulation of molecular vibrations [11], or coherent destruction of tunneling [3]. However, the first two mechanisms may heat or even destroy single-molecule devices, and the third mechanism requires strong fields. To overcome these difficulties, we propose a new type of single-molecule device, the phenyl-acetylene-macrocycle-based single-molecule transistor (PAM-SMT), which utilizes photon-assisted tunneling and destructive quantum interference (DQI).

Quantum interference is the key feature of coherent quantum transport, and DQI plays an essential role in the H-H tautomerization molecular switch [17] as well as the quantum interference effect transistor [18]. Recently, DQI has been experimentally observed in electron transport through a cross-conjugated molecular junction at room temperature [12]. Many theoretical studies on DQI involve ring-shaped conjugated molecules [4,18–23] or cross-conjugated molecules [24] due to their simple electronic structure and the proximity of their antiresonant states to the Fermi level of the electrodes. Moreover, *ab initio* calculations indicate that large conjugated molecules can enhance π-electron tunneling and suppress σ-electron tunneling [20]. On the basis of these studies and the consideration of synthetic feasibility, we choose benzene, davidene, and phenyl-acetylene macrocycle (PAM) [25,26] as candidate systems in Fig. 1. Amongst them we show below that PAM is the best system for single-molecule optoelectronic switch devices.

Photon-assisted tunneling has been extensively studied in superconductor-insulator-superconductor tunnel junctions [27] and semiconductor nanostructures [28,29] such as quantum dots [30,31]. However, until now photon-assisted tunneling in a single-molecule junction appeared to only be accessible in a system with weak hopping integrals, e.g., $\Delta \simeq 0.1$ eV [15], or in the presence of high-intensity fields, e.g., at $|\mathbf{E}| \simeq 2 \times 10^7$ V/cm [13,32]. The former regime is not reasonable for
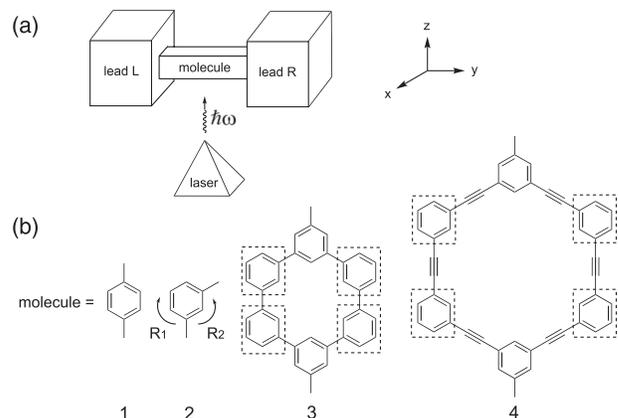

FIG. 1.   (a) The single-molecule optoelectronic device is made of two leads (source and drain electrodes), a single molecule, and a laser field (optical gate). (b) The candidate molecules are placed in the xy plane of the device. Molecule **1** (**2**) is benzene with a para- (meta-) connection forming the two leads; molecule **3** (**4**) is davidene (PAM) with a para- connection. Molecules **3** and **4** contain four identical building blocks, indicated by the dashed lines, based on the structure of molecule **2**, which offers two paths R_1 and R_2 with different lengths. For molecule **2**, Path R_1 has four carbon-carbon bonds, and the other path R_2 has two carbon-carbon bonds. In molecules **3** and **4**, combinations of R_1 and R_2 in the building blocks offer multiple pathways for controlled electron transport.

molecules; the latter domain could cause multiphoton excitation and possibly other undesirable processes. In this Letter, we show that it is feasible to measure photon-assisted tunneling in a single-molecule junction with a typical hopping integral in a weak laser field.

Model Hamiltonian.—The single-molecule optoelectronic device shown in Fig. 1(a) is described by the time-dependent Hamiltonian $H(t)$ composed of the external field-driven molecular Hamiltonian $H_{\mathrm{mol}}(t)$, the lead (electrode) Hamiltonian H_{lead}, and the molecule–lead coupling term H_{contact}. Within the Hückel model and the electric dipole approximation, the molecular Hamiltonian has the form $H_{\mathrm{mol}}(t) = \sum_n (E_0 - e\mathbf{r}_n \cdot \mathbf{E}(t))c_n^\dagger c_n + \sum_{n,n'} \Delta c_n^\dagger c_{n'}$, where $c_n^\dagger$ and c_n are Fermion operators which create and annihilate an electron in the p_z orbital $|n\rangle$ on the nth carbon at position $\mathbf{r}_n$ and $\mathbf{E}(t)$ is a time-dependent electric field. The values $E_0 = -6.553$ eV and $\Delta = -2.734$ eV are derived from photoelectron spectroscopy experiments [33]. The Hückel model is adequate for molecules **1**–**4** because their corresponding HOMO (highest occupied molecular orbital) and LUMO (lowest unoccupied molecular orbital) are linear combinations of p_z orbitals.

In addition, it is reasonable to neglect electron-phonon coupling in the molecular Hamiltonian because (a) molecules **1**–**4** have short chain length (< 2.2 nm) and large injection gaps (> 1.2 V) resulting in a small Landauer–Büttiker tunneling time (~ 1 fs) [34,35], and (b) experimental studies show that the conductance change caused by inelastic effects due to molecular vibrations is very small ($< 1\%$) under off-resonant conditions [36], and no significant variations of tunneling current caused by vibrationally induced decoherence appear at low bias ($\lesssim 0.2$ V) [37].

We use a noninteracting electron gas model to describe the two leads, $H_{\mathrm{lead}} = \sum_{lq} \epsilon_{lq} c_{lq}^\dagger c_{lq}$, where c_{lq} ($c_{lq}^\dagger$) annihilates (creates) an electron in the state $|lq\rangle$ with energy ϵ_{lq} in the lead l, and $l = L$ and R stand for the left and the right leads. Furthermore, assuming that the electrons in the leads are at equilibrium, their average occupation number can be expressed as $\langle c_{lq}^\dagger c_{l'q'} \rangle = \delta_{l,l'} \delta_{q,q'} f_l(\epsilon_{l,q})$, where $f_l(\epsilon) = (1 + e^{(\epsilon - \mu_l)/k_B\theta})^{-1}$ is the Fermi function of lead l with chemical potential μ_l at temperature θ. The molecule–lead couplings are modeled as $H_{\mathrm{contact}} = \sum_q V_{Lq,u} c_{Lq}^\dagger c_u + V_{Rq,v} c_{Rq}^\dagger c_v + \mathrm{H.c.}$, where $|u\rangle$ and $|v\rangle$ respectively represent the p_z orbital on the contact carbon atoms u and v, and the coupling function can be expressed as $\Gamma_{l,m} = 2\pi \sum_q |V_{lq,m}|^2 \delta(\epsilon - \epsilon_{lq})$, $(l, m) = (L, u)$ and (R, v).

Floquet analysis.—Consider molecules in a periodic time-dependent field $\mathbf{E}(t) = \mathbf{E}(t + T)$ with frequency $\omega = 2\pi/T$. By invoking Floquet theory [3,29], the underlying time-dependent Schrödinger equation can be cast into

$$\left(H_{\mathrm{mol}}(t) + \Sigma - i\hbar \frac{d}{dt}\right)|\phi_\alpha(t)\rangle = (\epsilon_\alpha - i\hbar\gamma_\alpha)|\phi_\alpha(t)\rangle, \quad (1)$$

where $|\phi_\alpha(t)\rangle = \sum_k |\phi_{\alpha,k}\rangle \exp(-ik\omega t)$ are the Floquet states and Σ is the self-energy arising from the leads. The Floquet eigenvectors $|\phi_\alpha(t)\rangle$ and their adjoint eigenvectors $|\phi_\alpha^\dagger(t)\rangle$ form a complete biorthogonal basis in Sambe space [38]. In Eq. (1), we only keep the imaginary part of the self-energy and set $\Sigma = \frac{-i}{2}(|u\rangle\Gamma_{L,u}\langle u| + |v\rangle\Gamma_{R,v}\langle v|)$ because the energy shift caused by the real part of the self-energy plays no role in the analysis.

The time-average current is computed using [3,29]

$$\bar{I} = \frac{2e}{h} \sum_{k=-\infty}^{+\infty} \int d\epsilon \{T_{RL}^{(k)}(\epsilon)f_L(\epsilon) - T_{LR}^{(k)}(\epsilon)f_R(\epsilon)\}, \quad (2)$$

where $T_{RL}^{(k)}(\epsilon) = \Gamma(\epsilon + k\hbar\omega)_{R,v}\Gamma(\epsilon)_{L,u}|G_{vu}^{(k)}(\epsilon)|^2$ is the transmission function of the tunneling electron from the left lead to the right lead with energy ϵ accompanied by k-photon absorption ($k > 0$) or emission ($k < 0$), and the factor of 2 comes from the spin degeneracy. The retarded Green function is

$$G_{vu}^{(k)}(\epsilon) = \sum_\alpha \sum_{k'=-\infty}^{+\infty} \frac{\langle v|\phi_{\alpha,k'+k}\rangle\langle\phi_{\alpha,k'}^\dagger|u\rangle}{\epsilon - (\epsilon_\alpha + k'\hbar\omega - i\hbar\gamma_\alpha)}. \quad (3)$$

In the wideband limit, assuming symmetric couplings $\Gamma(\epsilon)_{R,v} = \Gamma(\epsilon)_{L,u} = \Gamma$, the transmission function can be written as $T_{RL}^{(k)}(\epsilon) = \Gamma^2 |G_{vu}^{(k)}(\epsilon)|^2$ and $T_{LR}^{(k)}(\epsilon) = \Gamma^2 |G_{uv}^{(k)}(\epsilon)|^2$, in which $\Gamma = 0.5$ eV is a reasonable parameter for molecular devices [2,18].

Current without a laser field.—In the absence of the laser field, $T_{RL}^{(k)}(\epsilon) = T_{LR}^{(k)}(\epsilon) = \delta_{k,0}T(\epsilon)$ reduces Eq. (2) to the Landauer-type current formula [14], $\bar{I} = \frac{2e}{h} \int d\epsilon T(\epsilon)[f_L(\epsilon) - f_R(\epsilon)]$, which is employed to calculate the transmission for the four different types of conjugated molecules (Fig. 2). The transmission of molecules **2**, **3**, and **4** is strongly suppressed at energies $\epsilon = E_0 + \Delta$, E_0, and $E_0 - \Delta$ [21,23], in contrast to that of molecule **1**. The transmission suppression originates from DQI due to the tunneling electron following two paths of different length and can be understood by a free-electron network model [21]. It can be shown that DQI happens when the phase difference of the two paths satisfies $k_e 2d = \pi$, $2\pi/3$, and $4\pi/3$ [18,21] in the structure of molecule **2**, where d is the intersite distance of benzene and k_e is the de Broglie wave vector of the electron. The antiresonant states of molecules **2**–**4** happen at the same energies since all of them possess the same building blocks.

The repeated building blocks in PAM and molecule **3** operate like filters, which can suppress the transmission and broaden the range of antiresonance. For example, for PAM we found that, in the antiresonance range from -5.9 to -7.2 eV ($T < 10^{-10}$) and at a small source-drain voltage ($V_{SD} = 0.05$ V), the current is not experimentally detectable, e.g., $\bar{I} \approx eV_{SD}T/\pi\hbar = 3.87 \times 10^{-16}$ A at $T = 10^{-10}$. As a result, the extremely small transmission of molecule **3** and PAM is not sensitive to the Fermi level
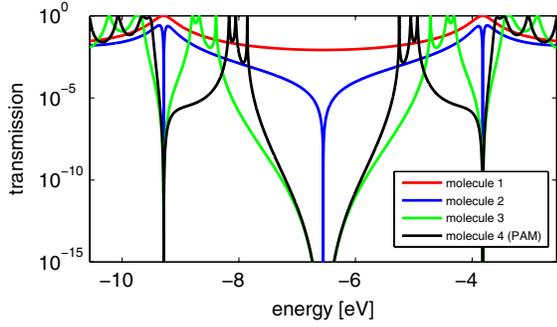
FIG. 2 (color online).   Transmission function of molecules **1**–**4** of Fig. 1 without a laser field for $\Gamma = 0.5$ eV, where the abscissa is the energy of the tunneling electron.

of the electrodes and functions as the *off state* of a single-molecule switch. Finally, we carried out geometry optimizations of isolated molecule **3** and PAM at the B3LYP/6-31 G(d) level using the GAUSSIAN 09 program [39] and found that only PAM has a stable planar conformation. Therefore, PAM is the best system for a single-molecule switch amongst molecules **1**–**4**. In addition, all peaks in Fig. 2 occur in pairs with opposite energies because all four molecules are alternant hydrocarbons [40]. The six peaks for PAM closest to $\epsilon = E_0$ correspond to MO 19–23 and MO 26–30 in Table I, respectively. The order of the MO 19–30 energies based on the Hückel model is consistent with the *ab initio* calculations [39]. The disappearance of MO 24 and MO 25 in Fig. 2 is due to the zero amplitude of the p_z orbital on the contact atoms, i.e., $\langle v|\phi_{\alpha,0}\rangle = \langle\phi_{\alpha,0}^{\dagger}|u\rangle = 0$.

Current in the presence of a laser field.—We assume that the monochromatic laser field is polarized in the y direction [see Fig. 1(a)]; thus, $e\mathbf{r}_n \cdot \mathbf{E}(t) = ey_nE\cos(\omega t)$, where y_n is obtained from the geometry optimization of PAM and E is the amplitude of the laser field. It can be shown that $T_{RL}^{(k)}(\epsilon) = T_{LR}^{(k)}(\epsilon)$ because the Floquet Hamiltonian of PAM satisfies a generalized parity symmetry $S_{GP} = (\mathbf{r}, t) \rightarrow (-\mathbf{r}, t + \pi/\omega)$ [15]. Consequently, we obtain the Landauer-type current formula $\bar{I} = \frac{2e}{h}\int d\epsilon T(\epsilon) \times [f_L(\epsilon) - f_R(\epsilon)]$ with $T(\epsilon) = \Gamma^2 \sum_{k=-\infty}^{\infty}|G_{vu}^{(k)}(\epsilon)|^2$.

The calculated transmission spectra of PAM are shown in Fig. 3(a), where the colors denote the magnitude of $T(\epsilon)$ on a logarithmic scale. Figure 3(b) is the profile of Fig. 3(a) at $\hbar\omega = 0.605$ eV. The lines in Fig. 3(a) and peaks in

TABLE I.   Molecular orbital (MO) energies of PAM based on the Hückel model calculation.

MO	Energy (eV)	MO	Energy (eV)
19	$\epsilon_{19} = -8.167$	25 (LUMO)	$\epsilon_{25} = -5.336$
20 and 21	$\epsilon_{20(21)} = -8.053$	26 and 27	$\epsilon_{26(27)} = -5.251$
22 and 23	$\epsilon_{22(23)} = -7.855$	28 and 29	$\epsilon_{28(29)} = -5.053$
24 (HOMO)	$\epsilon_{24} = -7.770$	30	$\epsilon_{30} = -4.939$

Fig. 3(b) correspond to tunneling involving different photon-assisted absorption or emission processes, e.g., $B1$–$B6$ for zero-photon tunneling, $B7$–$B12$ for one-photon assisted tunneling ($B7$–$B9$ and $B10$–$B12$ correspond to one-photon emission and absorption respectively), and $B13$–$B18$ for two-photon assisted tunneling. The coordinates of the intersection points in Fig. 3(a) can be expressed as $[(\epsilon_{a_1} - \epsilon_{a_2})/(k_2 - k_1), \epsilon_{a_1} + k_1(\epsilon_{a_1} - \epsilon_{a_2})/(k_2 - k_1)]$, where $a_{1(2)}$ denotes the $a_{1(2)}$th MO in Table I and $k_{1(2)}$ stands for the number of photons involved in the absorption and emission processes. For example, the intersection point of $B7$ ($a_1 = 30$, $k_1 = -1$) and $B12$ ($a_2 = 19$, $k_2 = 1$) is at $[\frac{1}{2}(\epsilon_{30} - \epsilon_{19}) = 1.614$ eV, $\frac{1}{2}(\epsilon_{30} + \epsilon_{19}) = -6.553$ eV]. Note that ϵ_{19} and ϵ_{30} lie, respectively, equally below and above E_0 so that $\frac{1}{2}(\epsilon_{30} + \epsilon_{19}) = E_0$. In addition, Fig. 3 shows that the transmission induced by one-photon assisted tunneling is much larger than that by two-photon assisted tunneling, which is reasonable at weak fields.

Consider the following experimental conditions for a single-molecule transistor. We assume a small source-drain voltage ($V_{SD} = 0.05$ V) and symmetric chemical potentials ($\mu_L = \mu + eV_{SD}/2$ and $\mu_R = \mu - eV_{SD}/2$).
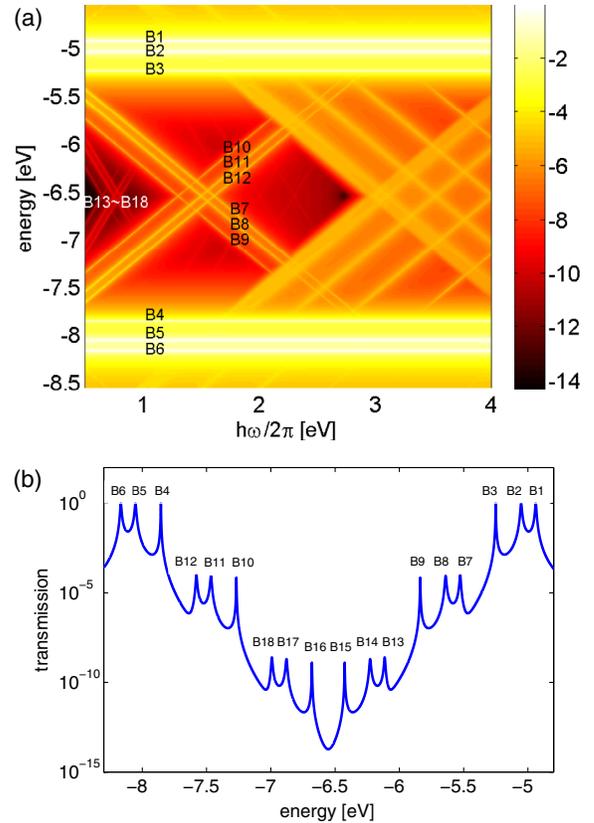

FIG. 3 (color online).   (a) Transmission spectra of PAM under laser fields for $E = 2 \times 10^5$ V/cm and $\Gamma = 0.5$ eV, where ω is the laser frequency and the colors denote the magnitude of transmission on a logarithmic scale; e.g., -2 stands for $T = 10^{-2}$. (b) Transmission spectrum at $\hbar\omega = 0.605$ eV.
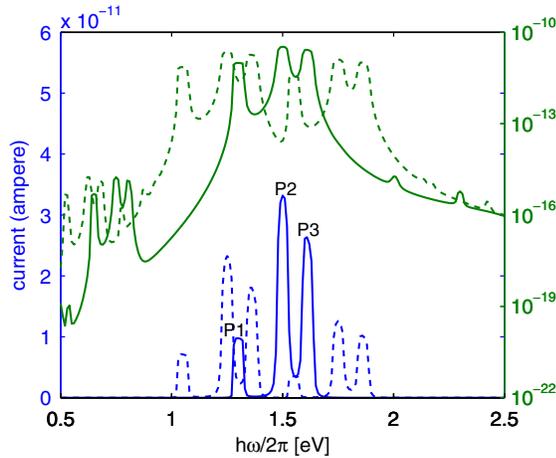
FIG. 4 (color online). Current-frequency characteristics of PAM for $V_{SD} = 0.05$ V, $k_B\theta = 5 \times 10^{-4}$ eV, $\Gamma = 0.5$ eV, and $E = 2 \times 10^5$ V/cm. The blue lines (lower set) show the magnitude of the current on a linear scale, and the green lines (upper set) show the same on a logarithmic scale. Solid lines are for $\mu = E_0$, and dashed lines are for $\mu = E_0 - 0.25$ eV, where μ is the zero-bias electrode chemical potential.

Figure 4 shows the current-frequency characteristics of PAM. Assuming that μ is located halfway between the HOMO and LUMO, i.e., $\mu = E_0$, we observe three peaks $P1$, $P2$, and $P3$ respectively at 1.30, 1.50, and 1.61 eV, which correspond to the intersection points of μ and one-photon quasistates in the transmission spectra [$B7$–$B12$ in Fig. 3(a)]. In addition, the frequencies of these peaks indicate the energy difference between the Fermi level of electrodes and the resonant-state energies of the single-molecule junction (for a small V_{SD}, Fermi level, $E_F \sim \mu$); i.e., the electronic structure of the molecular junction is revealed in the current-frequency characteristics. Moreover, the frequency range of $P1$–$P3$ is outside the regime of molecular vibrations (< 0.4 eV on the basis of frequency analysis at the PM6 level using the GAUSSIAN 09 program [39]) and electronic excitations (HOMO-LUMO gap $= 2.53$ eV), implying that the photon-assisted tunneling will not heat the molecules. Furthermore, the current response ($\sim 10^{-11}$ A) corresponding to a field strength of approximately 2×10^5 V/cm is detectable [41] and can cause large on–off current ratios (which can exceed 10^4), so photon-assisted tunneling can function as the *on state* of a single-molecule switch.

Assuming now that μ is not located halfway between the HOMO and LUMO, e.g., $\mu = E_0 - 0.25$ eV, the current caused by one-photon assisted tunneling is still distinctly observed in Fig. 4. The six peaks of the blue dashed line in Fig. 4 are located at 1.05, 1.25, 1.36, 1.55, 1.75, and 1.86 eV, which correspond to $B10$, $B11$, $B12$, $B9$, $B8$, and $B7$ in Fig. 3, respectively. Thus, the on state of PAM-SMTs is robust for electrodes with various chemical potentials.
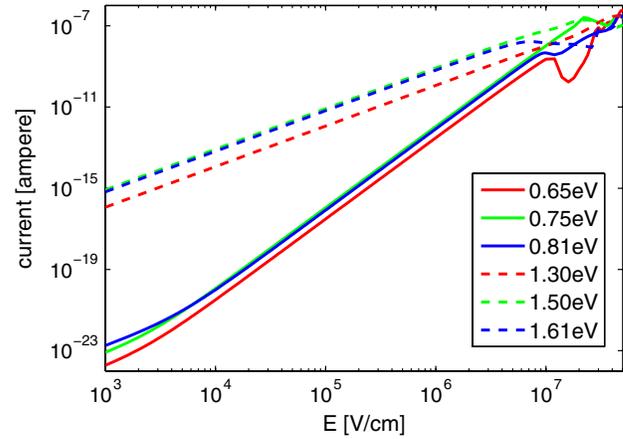

FIG. 5 (color online). Current-field intensity characteristics of PAM for $V_{SD} = 0.05$ V, $k_B\theta = 5 \times 10^{-4}$ eV, and $\Gamma = 0.5$ eV, where each line shows the current in a laser field with a particular frequency. Solid lines and dashed lines correspond to currents induced by two-photon assisted tunneling and one-photon assisted tunneling, respectively.

Two-photon assisted tunneling also can be observed in the field frequency range from 0.5 to 1 eV. Figure 5 shows that the current induced by two-photon assisted tunneling is proportional to the fourth power of the field amplitude E in the range from 10^4 to 2×10^6 V/cm, while the current induced by one-photon assisted tunneling is proportional to the second power of E for $E < 2 \times 10^6$ V/cm. The proportionality can be understood from a perturbation analysis, assuming that the electric-dipole term in $H(t)$ is small such that the one-photon Green's function $G_{vu}^{(\pm 1)}(\epsilon)$ in the Landauer formula is proportional to E and the two-photon Green's function $G_{vu}^{(\pm 2)}(\epsilon)$ is proportional to E^2, respectively. These field amplitude power laws can be used to examine one-photon and two-photon assisted tunneling in single-molecule devices. For field amplitudes satisfying $E \gtrsim 2 \times 10^6$ V/cm, the simple power laws no longer hold due to Stark shifting of the quasistates. The deviation of the solid lines from the power law behavior in the regime of $E \lesssim 10^4$ V/cm is due to the overlap of two-photon and one-photon assisted tunneling. Figure 5 depicts the effective range of field intensity for photon-assisted tunneling in PAM-SMTs.

In conclusion, we have presented a general principle for operating a single-molecule switch based on PAM-SMTs. The results imply that a molecule with a wide and strong antiresonance near the Fermi level of the electrodes should be a good candidate for a single-molecule optoelectronic switch. Our computations show that the strong transmission suppression of PAM in a simple Hückel model can be carried over to (a) an extended Hückel model which includes all valence orbitals and long-range hopping [2] and (b) a self-consistent-field Pariser–Parr–Pople model which includes electron–electron interactions [18]. The computational results for these latter two models are not shown here

since the Hückel model is sufficient to describe the physical phenomenon of DQI in PAM-SMTs. Finally, the results here open up a new class of molecular switches for experimental study and theoretical investigation including additional physical issues, e.g., asymmetric molecule–lead coupling [15], electron–phonon coupling [16], and other dephasing processes.

*hrabitz@princeton.edu

[1] V. Mujica, M. Kemp, and M. A. Ratner, J. Chem. Phys. **101,** 6849 (1994)

[2] W. Tian, S. Datta, S. Hong, R. Reifenberger, J. I. Henderson, and C. P. Kubiak, J. Chem. Phys. **109,** 2874 (1998).

[3] S. Camalet, J. Lehmann, S. Kohler, and P. Hänggi, Phys. Rev. Lett. **90,** 210602 (2003).

[4] J. Rincón, K. Hallberg, A. A. Aligia, and S. Ramasesha, Phys. Rev. Lett. **103,** 266807 (2009).

[5] J.-T. Lü, P. Hedegård, and M. Brandbyge, Phys. Rev. Lett. **107,** 046801 (2011).

[6] M. A. Reed, C. Zhou, C. J. Muller, T. P. Burgin, and J. M. Tour, Science **278,** 252 (1997).

[7] J. Park et al., Nature (London) **417,** 722 (2002).

[8] S. J. van der Molen, J. Liao, T. Kudernac, J. S. Agustsson, L. Bernard, M. Calame, B. J. van Wees, B. L. Feringa, and C. Schonenberger, Nano Lett. **9,** 76 (2009).

[9] H. Song, Y. Kim, Y. H. Jang, H. Jeong, M. A. Reed, and T. Lee, Nature (London) **462,** 1039 (2009).

[10] J. J. Parks et al., Science **328,** 1370 (2010).

[11] Z. Liu et al., Nature Commun. **2,** 305 (2011).

[12] C. M. Guédon, H. Valkenier, T. Markussen, K. S. Thygesen, J. C. Hummelen, and S. J. van der Molen, Nature Nanotech. **7,** 305 (2012).

[13] A. Tikhonov, R. D. Coalson, and Y. Dahnovsky, J. Chem. Phys. **116,** 10 909 (2002).

[14] S. Camalet, S. Kohler, and P. Hänggi, Phys. Rev. B **70,** 155326 (2004).

[15] J. Lehmann, S. Kohler, and P. Hänggi, J. Chem. Phys. **118,** 3283 (2003).

[16] J. Lehmann, S. Kohler, V. May, and P. Hänggi, J. Chem. Phys. **121,** 2278 (2004).

[17] J. Prasongkit, A. Grigoriev, R. Ahuja, and G. Wendin, Phys. Rev. B **84,** 165437 (2011).

[18] D. M. Cardamone, C. A. Stafford, and S. Mazumder, Nano Lett. **6,** 2422 (2006).

[19] S. Sautet and C. Joachim, Chem. Phys. Lett. **153,** 511 (1988).

[20] S. H. Ke and W. T. Yang, Nano Lett. **8,** 3257 (2008).

[21] L.-Y. Hsu and B.-Y. Jin, Chem. Phys. **355,** 177 (2009).

[22] Y. Tsuji, A. Staykov, and K. Yoshizawa, J. Am. Chem. Soc. **133,** 5955 (2011).

[23] T. Hansen, G. C. Solomon, D. Q. Andrews, and M. A. Ratner, J. Chem. Phys. **131,** 194704 (2009).

[24] G. C. Solomon, D. Q. Andrews, R. H. Goldsmith, T. Hansen, M. R. Wasielewski, R. P. Van Duyne, and M. A. Ratner, J. Am. Chem. Soc. **130,** 17 301 (2008).

[25] M. M. Haley, J. J. Pak, and S. C. Brand, Top. Curr. Chem. **201,** 81 (1999).

[26] A. S. Shetty, J. Zhang, and J. S. Moore, J. Am. Chem. Soc. **118,** 1019 (1996).

[27] P. K. Tien and J. P. Gordon, Phys. Rev. **129,** 647 (1963).

[28] G. Platero and R. Aguado, Phys. Rep. **395,** 1 (2004).

[29] S. Kohler, J. Lehmann, P. Hänggi, Phys. Rep. **406,** 379 (2005).

[30] C. A. Stafford and N. S. Wingreen, Phys. Rev. Lett. **76,** 1916 (1996).

[31] T.-S. Ho, S.-H. Hung, H.-T. Chen, and S.-I. Chu, Phys. Rev. B **79,** 235323 (2009).

[32] A. Tikhonov, R. D. Coalson, and Y. Dahnovsky, J. Chem. Phys. **117,** 567 (2002).

[33] J. P. Lowe and K. A. Peterson, Quantum Chemistry (Elsevier, New York, 2006).

[34] A. Nitzan, J. Jortner, J. Wilkie, A. L. Burin, and M. Ratner, J. Phys. Chem. B **104,** 5661 (2000).

[35] A. Nitzan, Annu. Rev. Phys. Chem. **52,** 681 (2001).

[36] H. Song, Y. Kim, H. Jeong, M. A. Reed, and T. Lee, J. Phys. Chem. C **114,** 20 431 (2010).

[37] S. Ballmann, R. Härtle, P. B. Coto, M. Elbing, M. Mayor, M. R. Bryce, M. Thoss, and H. B. Weber, Phys. Rev. Lett. **109,** 056801 (2012).

[38] H. Sambe, Phys. Rev. A **7,** 2203 (1973).

[39] M. J. Frisch et al., GAUSSIAN 09, revision A.02, Gaussian, Inc. (Wallingford, CT, 2009).

[40] L. Salem, The Molecular Orbital Theory of Conjugated Systems (W. A. Benjamin, Inc., New York, 1966).

[41] Y.-S. Chen, M.-Y. Hong, and G.-S. Huang, Nature Nanotech. **7,** 197 (2012).